

Chaos and Regularity in Semiconductor Microcavities

Hichem Eleuch^{1,2} and Awadhesh Prasad^{1,3*}

¹*Max Planck Institute for the Physics of Complex Systems,
Nöthnitzer Str. 38, 01187 Dresden, Germany*

²*Institute for Quantum Science and Engineering,
Texas A & M University,*

College Station, Texas 77843, USA

³*Department of Physics and Astrophysics,
University of Delhi, Delhi 110007, India*

Our work presents a study on the nonlinear dynamical behavior for a microcavity semiconductor containing a quantum well. Using an external periodic perturbation in energy level we observe the periodic-doubling, quasiperiodic, and direct route to chaos as forcing strength is changed. For a particular case the riddled basin for coexisting periodic and chaotic motions are observed. These results suggest that the dynamics of exciton-photon is quite complex in presence of external perturbation.

PACS numbers: 71.35.Gg, 05.45.-a, 05.45.Pq, 05.45.Ac

Keywords: Semiconductor Microcavity, Exciton-mediated interaction, Multistability, Riddling, Chaos

I. INTRODUCTION

The properties of the light emitted from a quantum well exciton embedded in semiconductor microcavities have drawn attention of several theoretical and experimental researchers in the last twenty years [1–11], given their potential application in opto-electronic devices [12, 13]. Phenomena which are linked to quantum electrodynamics, such as Rabi splitting and Autler-Townes doublets, have been observed [5, 14, 15].

In the strong coupling regime when the coupling frequency between the exciton and photon is larger than the relaxation frequencies of the medium and the cavity, the vacuum Rabi splitting has been observed. The degeneracy between the cavity resonance and the medium is lifted and two lines appear in the intensity spectrum of the exciton-cavity system. Semiconductor quantum wells exhibiting narrow absorption lines corresponding to excitonic strengths of these resonances make it possible to achieve the strong coupling regime and to observe the vacuum Rabi splitting. In the strong coupling regime also, modifications of quantum statistical properties of the emitted light, were theoretical predicted and experimentally proved [6, 16–21]. In 2004, the group of Giacobino proved the existence of the optical bistability in the semiconductor microcavities [22]. Bistability occurs when there exist two possible stable states for the same set of system parameters. Optical bistability can play a major role for the conception of the optical memories paving the way to the realization of the quantum computer.

Recently, multistability in semiconductor QED systems in the strong coupling regime was observed in different experiments [23, 24]. The multistability can arise due to different effect such as polarization-dependent nonlinear interactions [23] or thermal induced processes [25].

Either in natural systems or in experimental realizations the presence of an external forcing is unavoidable. Such external forcing could be either noise (either from surroundings or inherent within the experiment) or deterministic perturbation. The external forcing in nonlinear dynamical systems has been extensively studied. This forcing sometimes gives important and useful results e.g. stochastic resonances [26, 27], chaos control [28, 29], strange nonchaotic dynamics [30–32] etc. One aspect for exploring the nonlinear behavior is to scan the parameters space and observe how the dynamical complexity depends on the parameters [33–36]. For a given set of parameters understanding the basins of coexisting attractors are also equally important, particularly, when there are riddled basins [37–40]. The aim of this Letter is to analyze the dynamical behaviors (particularly routes to chaos [33–36] and riddling [37–40]) of the intra-cavity photonic intensity and the intensity of the florescent light in the presence of periodic signals.

In this work we explore the dynamics of the field intensities for high excitation regime inside a semiconductor microcavity containing a quantum well. We observe that the periodic-doubling, quasiperiodic and direct route chaos as forcing strength is being changed. This shows the existence of various types of dynamics over the forcing strengths. Furthermore coexisting periodic and chaotic attractors are also observed with riddled basin.

* Corresponding Author: Email- awadhesh@physics.du.ac.in, Telephone +49 351 8712125, Fax +49 351 8711999.

The paper is organized as follows. In Sec. II, we review the derivation of exciton-phonon interaction. This is followed in Sec. III by results and discussion for three particular cases of detuning where various complex dynamics are presented. Results are concluded in Sec. IV.

II. MODEL

We consider a microcavity, containing a semiconductor quantum well, with width of the order of the wavelength λ . The quantum well is localized in a position, which corresponds to the maximum of the electromagnetic field. This system is described in detail in [41].

Our discussions are limited to the semiconductors with two bands. The electromagnetic field can excite an electron of the valence band to the conduction band by creating a hole in the valence band. The electron and the hole interact by giving excitonic states, which are similar dependent states to the states of hydrogen atoms. The state 1S which is the low bound state (fundamental state) has the greatest oscillator strength. It is for this reason that this processing of the interaction between exciton - photon often takes into account only this state. Neglecting the effects of the spins and the interaction with the phonons we can write a Hamiltonian describing the system [42–44]:

$$\begin{aligned}
H = & \sum_{k_{//}} \hbar \omega_{k, \text{photon}} a_{k_{//}}^+ a_{k_{//}} + \sum_{K_{//}} \hbar \omega_K b_{k_{//}}^+ b_{k_{//}} + \sum_{k_{//}} \hbar g_{k_{//}} \left(a_{k_{//}}^+ b_{K_{//}} + b_{K_{//}}^+ a_{k_{//}} \right) + \\
& + \frac{1}{2} \sum_{K_{//}, K'_{//}, q} V_q^{eff} b_{K_{//}+q}^+ b_{K'_{//}-q}^+ b_{k_{K_{//}}} b_{K'_{//}} \\
& - \sum_{K_{//}, K'_{//}, q} \frac{\hbar g_{k_{//}}}{n_{sat}} A a_{k_{//}+q}^+ b_{K'_{//}-q}^+ b_{k_{//}} b_{K'_{//}} + h.c.
\end{aligned} \tag{1}$$

The photonic and excitonic modes are quantified according to the normal direction to the microcavity. The vectors of waves are thus vectors parallel with the planes of the layers. In a perfect planar cavity, the invariance by translation imposes that the exciton with parallel wave vector can couple only with the same photons with parallel wave vector $k_{//} = K_{//}$.

The first two terms of the Hamiltonian correspond to the proper energies of photon and exciton, where $a_{k_{//}}$, $b_{K_{//}}$ are respectively the annihilation operators of a photonic and excitonic mode verifying:

$$\left[a_{k_{//}} , a_{k'_{//}}^+ \right] = \delta_{k_{//} k'_{//}} \tag{2}$$

$$\left[b_{k_{//}} , b_{k'_{//}}^+ \right] = \delta_{k_{//} k'_{//}} \tag{3}$$

$\omega_{exc, K_{//}}$, $\omega_{ph, k_{//}}$ are the photonic mode and excitonic mode frequencies of the cavity. The third term corresponds to the exciton-photon coupling with a coupling constant g . This constant is a function of the oscillator strength by unit of area $\frac{f}{S}$, the effective length of the cavity L_c , the dielectric permeability ε , the mass m_0 and the free electron charge e [45]:

$$g = \sqrt{\frac{f}{2m_0 \varepsilon L_c S}} \tag{4}$$

and the fourth term represents the saturation of the interaction photon-exciton due to the fermionic nature of the electrons and the Holes, with [43, 44, 46, 47]:

$$n_{sat} = \frac{7}{16\pi\lambda_x^2} \tag{5}$$

λ_x being the radius of Bohr of the bidimensional exciton and it is about $100\overset{\circ}{\text{Å}}$ in the GaAs microcavity with a quantum well.

The last term describes the interaction between exciton due to the Coulomb interaction between components of an exciton and those of a neighboring exciton. The effective potential is given by:

$$V_q^{eff} = V_0^{eff} \approx \frac{6e^2}{\varepsilon A} \lambda_x \quad (6)$$

where A is the surface of quantification. We limit ourselves to the case of a pumping having a normal incidence and which results in the excitation of only one photonic mode of the cavity with wave vector $q = 0$.

The momentum conservation imposes that this photonic mode is coupled only with only one excitonic mode $K_{//} = 0$. The Hamiltonian describing exciton in the microcavity with a quantum well interacting with the photons is then:

$$H = \hbar\omega_{ph}a^+a + \hbar\omega_{exc}b^+b + i\hbar g (a^+b - b^+a) + \frac{1}{2}V_0b^+b^+bb - \frac{\hbar g}{n_{sat}} (a^+b^+bb + b^+b^+ab). \quad (7)$$

If the excitation is very weak which correspond to very low density, the distance which separates one exciton from its neighbor is very large so that the interaction between excitons is negligible as well as the effects of saturation and the exciton can be considered as a pure boson and the exciton-photon interaction can be modeled like an interaction between two harmonic oscillators [48–50]:

$$H_{lin} = \hbar\omega_{ph}a^+a + \hbar\omega_{exc}b^+b + \hbar g (a^+b + b^+a). \quad (8)$$

The third term of this Hamiltonian indicates the coupling between exciton-photon and represent the exchange of excitations. The term a^+b describes the creation of a photon and the annihilation of an exciton and the term ab^+ describes the creation of an exciton and the annihilation of a photon. The proper states of this system are called polariton states of the cavity. The diagonalization of the Hamiltonian gives energies E_+ and E_- of polaritons in the cavity:

$$E_{\pm} = \frac{E_{cav} + E_{ex}}{2} \pm \frac{\hbar\Delta}{2} \quad (9)$$

with

$$\Delta = \sqrt{\delta_1^2 + 4g^2} \quad (10)$$

where the difference of frequency between frequencies of exciton and photon:

$$\delta_1 = \omega_{cav} - \omega_{exc}. \quad (11)$$

The corresponding polariton operators P_{\pm} are linear combinations of the excitonic and photonic operators:

$$P_- = Xb - Ca \quad (12)$$

$$P_+ = Cb - Xa \quad (13)$$

with X and C are the Hopfield coefficients:

$$X = \frac{\delta_1 + \Delta}{\sqrt{2\Delta(\delta_1 + \Delta)}} \\ C = \frac{2g}{\sqrt{2\Delta(\delta_1 + \Delta)}}. \quad (14)$$

If we take into account the relaxation phenomena due to the finished lifetime of excitons and photons that can be explained by the dissipations of the cavity (γ_{cav}) and that of the exciton γ_{exc} .

We can modalize these effects by introducing the complex energies for the exciton $E_{cav} - i\hbar\gamma_{cav}$ and for the photon of the cavity $E_{exc} - i\hbar\gamma_{exc}$ [12]. Then we get complex energies whose real part gives the energy of polariton and the imaginary part represents the rates of polariton relaxation:

$$E_{\pm} = \frac{E_{cav} + E_{exc}}{2} - i\hbar \frac{\gamma_{cav} + \gamma_{exc}}{2} \pm \frac{\hbar\Delta}{2} \quad (15)$$

$$\Delta^2 = (\delta_1 - \hbar(\gamma_{cav} - \gamma_{exc}))^2 + 4g^2. \quad (16)$$

The polariton relaxation rates for the upper and lower branches are [48] :

$$\begin{aligned} \gamma_+ &= \gamma_{exc} \cos^2(\Theta) + \gamma_{cav} \sin^2(\Theta) \\ \gamma_- &= \gamma_{exc} \sin^2(\Theta) + \gamma_{cav} \cos^2(\Theta) \end{aligned} \quad (17)$$

where Θ is the coupling angle defined by :

$$tg(2\Theta) = \frac{-g}{2(\omega_{cav} - \omega_{ex})} = \frac{g}{2\delta_1}. \quad (18)$$

In the case where the exciton and the cavity are in the resonance ($\omega_{cav} = \omega_{ex}$) dissipations of the two branches are equal to the average of excitonic and photonic dissipations:

$$\gamma_+ = \gamma_- = \frac{\gamma_{exc} + \gamma_{cav}}{2}. \quad (19)$$

If we take into account the effects of nonlinearity due to the excitonic interactions and the effects of saturation we must reconsider the fourth and fifth terms of the global Hamiltonian H .

Let us now derive the evolution of the excitonic and photonic fields in the non linear regime where the density of exciton is high. The evolution of the mean field operators in the interaction picture, by considering that the fluctuations are weak compared to the average values, can be written as:

$$\frac{d\langle a \rangle}{d\tau} = \varepsilon(t) + g\langle b \rangle - \kappa\langle a \rangle - i\Delta_a\langle a \rangle \quad (20a)$$

$$\frac{d\langle b \rangle}{d\tau} = -g\langle a \rangle - \frac{\gamma}{2}\langle b \rangle - i\Delta_b\langle b \rangle - 2i\alpha\langle b^+ \rangle\langle b \rangle\langle b \rangle \quad (20b)$$

$$\frac{d\langle a^+ \rangle}{d\tau} = \varepsilon(t) + g\langle b^+ \rangle - \kappa\langle a^+ \rangle + i\Delta_a\langle a^+ \rangle \quad (20c)$$

$$\frac{d\langle b^+ \rangle}{d\tau} = -g\langle a^+ \rangle - \frac{\gamma}{2}\langle b^+ \rangle + i\Delta_b\langle b^+ \rangle + 2i\alpha\langle b^+ \rangle\langle b^+ \rangle\langle b \rangle \quad (20d)$$

where τ is a dimensionless time normalized to the round trip time τ_c in the cavity:

$$\tau = \frac{t}{\tau_c}$$

γ , κ are the dimensionless decay rates of the exciton and cavity photon:

$$\gamma = \gamma_{ex} \tau_c; \kappa = \gamma_{ph} \tau_c$$

the nonlinear coupling constant is normalized to $\frac{1}{\tau_c}$:

$$\alpha = \left(\frac{4g}{n_{sat}} X^3 C + \frac{V_0}{\hbar} X^4 \right) \tau_c \quad (21)$$

and Δ_a, Δ_b are the dimensionless detuning

$$\begin{aligned} \Delta_a &= (\omega_{ph} - \omega_L) \tau_c \\ \Delta_b &= (\omega_{ex} - \omega_L) \tau_c. \end{aligned} \quad (22)$$

As this system is already 4-dimensional and hence the presence of forcing makes the system more complex and difficult to understand it analytically. Therefore the numerical simulation is used to uncover the various dynamical states using RK4 integrator [51]. We consider the step size $\Delta t = 2\pi/5000$ for integration. The dynamical studies are studied after removing initial 10^7 data points as transients. We explore here the photon and exciton intensities $I_a = \langle a^+ \rangle \langle a \rangle$ and $I_b = \langle b^+ \rangle \langle b \rangle$ inside the cavity. As the fluorescent light is proportional to the mean number of excitons (I_b), we are also exploring the fluorescent light dynamics.

III. RESULTS AND DISCUSSIONS

There are various physical parameters in this system. We fix the normalized parameters by $g = 1.5$, $\kappa = 0.12$, $\gamma = 0.015$. These parameters correspond to the experimental values [22] in units of the inverse of the round-trip in the microcavity. We concentrate our analysis to the strong pump field where the non-linear phenomenon exhibits interesting dynamics, in this case we choose a normalized amplitude of laser pump $\epsilon = 200$ and the normalized excitonic interaction coefficient $\alpha = 0.00001$. At this set of parameters the system has stable fixed point solution. However, particularly ϵ is more prone to external influence. Therefore in this study we consider this parameter only to observe the effect of the external forcing. In this work we restrict our analysis to the deterministic periodic forcing in ϵ i.e. $\epsilon : \epsilon = 1 + f \cos(\Omega t)$ where Ω is the perturbation frequency while f is the strength of the forcing which is considered as bifurcation parameter [52]. It is clear that for $f = 0$ the motion is fixed point solution. As we change the magnitude of f , various dynamical motions are possible which we will discuss below for different values of the detuning Δ_a and Δ_b . We limit our study to the case of the resonance between the exciton and the cavity $\omega_{ex} = \omega_{ph}$. In the strong regime where the values of the dissipation rates γ and κ are small compared to the coupling constant exciton-photon g , the systems exhibits two polaritonic branches at $\omega_{ex} \pm g$ (see Eq. (15)). We explore the dynamics for these two cases where the laser pump is resonant to one of the polaritonic frequencies $\Delta_a = \Delta_b = \pm g$. We also analyze the case of the total resonance between the cavity, laser pump and the exciton $\Delta_a = \Delta_b = 0$.

A. Case-I: .

Let us begin with the case of total resonance $\Delta_a = \Delta_b = 0$. Shown in Fig. 1(a) is the spectrum of Lyapunov exponents (LE), λ_i [33] as function of forcing strength f . The variation of LEs indicates the different dynamical states as the forcing strength f is changed. Here the zero Lyapunov exponent is plotted as a dotted (blue) line while largest two non-zero Lyapunov exponents are plotted as solid (black) and dashed (red) lines. The figures in middle row represent the intensity of the photons inside the cavity $I_a = \langle a^+ \rangle \langle a \rangle$ (black-solid line) and the intracavity excitonic intensity $I_b = \langle b^+ \rangle \langle b \rangle$ (red-dashed line) as function of time at different values of the forcing strengths (b) $f = 0.1$, (c) $f = 0.804$ (d) 0.329, and (e) 0.5 which present the different dynamical motions as period-one, period-six, quasiperiodic (QP) and chaotic (C) respectively. These different dynamical motions can be further confirmed by Poincaré section [33] taken at $Re < a > = 0$, as shown in lowest row. The respective motions are the period-one (single point), period-six (six points), quasiperiodic (closed curve) and chaotic (scattered points). These results clearly demonstrate that there are various possible dynamical states which depend on the forcing strength.

As the forcing f increased from zero, the motion goes from periodic (P) to chaotic via QP. The left inset figure of Fig. 1 shows the expanded region in near to the transition marked as F_1 . It clearly indicates that the motion goes from periodic to chaotic via quasiperiodic where two Lyapunov exponents are zero. This transition can be termed as quasiperiodic route to chaos, a route which has been found is generic in many other dissipative dynamical systems [34–36]. Near to the transition F_2 there is an another route to chaos where the periodic motion gets doubled and leads to chaos as the forcing parameter is being increased. This is clearly shown in an expanded Fig. 2 (a) which demonstrates that whenever the largest non-zero Lyapunov exponent reaches to the zero value, the period gets doubled. This period doubling is further confirmed in Fig. 2 where 100 consecutive maxima of $Re < a >$ (at a fixed

parameter) is plotted as a function of forcing parameter. Here the periods get bifurcated as periods $6 \rightarrow 12 \rightarrow 24 \dots$. A representative period-six motion is shown in Figs. 1(c) and (g). Apart from these transitions there are many other periodic windows, e.g. F_4, F_5, F_7 etc. where one of the above routes occurs.

However as the forcing strength f is decreased near the marked transition F_3 , the motion becomes chaotic from periodic where there is sudden jump in Lyapunov exponents. This suggests that there is direct transition from periodic to chaotic as shown in inset figure near to the transition F_3 . This suggest that this is an another type of route to chaos. Here due to high dimensionality of the system it is difficult to find the normal form to understand the exact type of bifurcation. Apart from the above routes/dynamics there are various periodic windows of different periods also e.g. near to F_4 . These results indicate that in the presence of the external forcing this system exhibits various type of dynamics.

B. Case-II: $\Delta_a = \Delta_b = g$

This situation presents the case where the laser pump is resonant to the upper polaritonic branch. Similar to the case-I, we plot in Fig. 3 (a) the largest two Lyapunov exponents, λ_i as a function of the forcing strength f . The figures in middle row show the intensities I_a (black-solid line) and I_b (red-dashed line) as a function of time at different forcing strengths (b) $f = 0.06$, (c) 0.18 and (d) 0.8 for periodic, quasiperiodic, and chaotic attractors respectively. These different dynamical motions can be further confirmed by Poincaré section taken at $Re < a > = 0$, as shown in lowest row, for respective motions which are the period-one (single point), quasiperiodic (closed curve) and chaotic (scattered points) motions. These clearly demonstrate that these various dynamical states also possible in this case as well.

Here as the forcing strength is increased from zero, the period motion becomes quasiperiodic (which is in wider region than that of the Case-I) and then is chaotic near to the transition F_1 . Here also the transition F_1 where motion goes from periodic to chaotic is direct in the sense that the periodic motion suddenly becomes chaotic. This transition, similar to F_3 transition in Case-I, is still not exactly clear due to inability to get its normal form.

C. Case-III: $\Delta_a = \Delta_b = -g$

This situation presents the case where we pump resonantly to the lower polaritonic branch. In Fig. 4 (a) are plotted the spectrum of Lyapunov exponents, λ_i as a function of the forcing strength f . Similar to Figs. 1 and 3 shown in middle row are the intensities I_a (black-solid line) and I_b (red-dashed line) as function of time at different forcing strengths (b) $f = 0.5$ and (d) 1.7728 for periodic and chaotic attractors respectively. The corresponding Poincaré sections, taken at $Re < a > = 0$, are shown in lowest row, which confirm the period-one (single point), and chaotic (scattered points) motions respectively. These clearly demonstrate that, in this case as well, various dynamical states are also possible.

However the transition from periodic to chaotic and then to periodic is quite different than from the previous Cases-I and II. Here we don't find neither period-doubling nor quasiperiodic nor direct route to chaos as observed in previous cases. A remarkable feature of this case is that there appears to be a parameter interval, near the transition F_1 in Fig. 4(a), where the system exhibits wild fluctuations as a function of the forcing strength f . These fluctuations persist on small scales, as shown in a blowup of marked box in inset figure. Such fluctuations typically indicate co-existing attractors with complicated basins [37–40] because of a small change in the parameter f , it can lead to a completely different attractor. Here we do observed coexisting periodic (Fig. 5(a)) and chaotic (Fig. 5(b)) motions. The basin of these multistable attractors are shown Fig. 5(c) with different initial conditions corresponding to periodic (open circles) and chaotic (star) motions. In the diagonal region, interwoven initial conditions show the presence of complicated basins where both of the attractors coexist. In order to confirm the complicated basins, it is plotted in Fig. 5(c) the basin of expanded region of marked box in (d). This demonstrate that basin is riddled [37–40] i.e. if an initial condition goes to periodic attractor then for any slight change in the f parameter, say within the change δ , it may go to chaotic attractor, and vice-versa. However, this phenomenon of riddling can be verified via the computation of an uncertainty exponent. Fixing a perturbation, δ , and randomly choosing a pair of systems within a region, the parameters are termed uncertain if they yield different asymptotic states. The fraction of uncertain parameter pairs, $q(\delta)$, typically decreases with δ as a power

$$q(\delta) \propto \delta^\beta$$

which defines the uncertainty exponent β [37–40]. Results are plotted in Fig. 5(e) where the exponent is approximately zero (the best fit to the data yields $\beta = 0.0008 \pm 0.0004$) which is typical of riddle or riddle-like basins

[37–40]. The practical implication is that in this region, the attractor cannot be predicted no matter how small the uncertainty in the specification of parameters. This suggests that this system exhibits complicated dynamics which not only depends on initial conditions but also on the perturbation parameter.

IV. CONCLUSION

In summary, we have studied the dynamical behavior of the photonic and excitonic intensities inside a semiconductor microcavity with a quantum well. As the fluorescent light is proportional to the intracavity excitonic intensity, we have explored also the fluorescent light dynamics.

We have observed first that by varying the external perturbation we can change the intracavity field intensities. By increasing the amplitude of the external perturbation f and independently of the resonance configurations mainly the photon intensity inside the cavity is increased.

By pumping the upper polaritonic branch (caseII) there are more excitons than photons inside the cavity and by pumping the lower polaritonic branch (case III) we have the inverse situation (see Figs. 2 and 3). This can be interpreted by the fact that excitonic nonlinearity induces more excitons in the upper branch than in the lower one. The enhancement of the photon intensity is more pronounced by pumping resonantly to the upper polaritonic branch.

A modification of the trajectory regularity is observed by increasing the external forcing strength f . As shown in Fig 1,2 and 3, by increasing the perturbation amplitude f the dynamics of the system changes from stable point (Fig. 1a, Fig. 2a, Fig. 3a) to chaotic motion (Fig. 1c, Fig. 2c and Fig. 3c). The quasiperiodic motion is totally absent in the case III. Moreover the basin of attractor in III are quite complicated.

The Case-III shows different behavior in comparison to I and II. The chaos is observed in wide range of parameters for I and II. From this we can conclude that the regularity of the dynamics for the polaritonic lower branch is less sensitive to the external perturbation. Furthermore we have observed that Hyper chaotic behavior (more that one Lyapunov exponents are rather that zero) in I but not in II and III. This means that by pumping in the middle between the two polaritonic branches the system presents very complex dynamics. In addition, we can deduce that the perturbation affects less the polaritonic lower branch than the upper branch(see Figs. 2 and 3). By pumping with a laser frequency detuned from the polaritonic frequencies the system exhibits high sensitivity to the perturbations. This effect can originate from the nonlinear effects induced by the exciton-exciton interaction. The nonlinearity affects more the frequency ranges detuned from the polaritonic frequencies and induces high dependence of the system to the external perturbations.

Acknowledgements

The authors thank E. Siminos for valuable comments and acknowledge the financial support and the hospitality of MPIPKS.

-
- [1] A. L. Bradley, J. P. Doran, T. Aherne, J. Hegarty, R. P. Stanley, R. Houdré, U. Oesterle, and M. Ilegems, *Phys. Rev. B* **57**, (1998) 9957.
 - [2] A. Amo, D. Sanvitto, F. P. Laussy, D. Ballarini, E. del Valle, M. D. Martin, A. Lemaitre, J. Bloch, D. N. Krizhanovskii, M. S. Skolnick, C. Tejedor and L. Vina, *Nature* **457**, (2009) 291-295.
 - [3] D. D. Solnyshkov, R. Johne, I. A. Shelykh, and G. Malpuech, *Phys. Rev. B* **80**, (2009) 235303.
 - [4] G. Khitrova, H.M. Gibbs, M. Khira, S.W. Koch, A. Scherer, *Nature Phys.* **2**, (2006) 81.
 - [5] C. Weisbuch, M. Nishioka, A. Ishikawa, and Y. Arakawa, *Phys. Rev. Lett.* **69**, (1992) 3314.
 - [6] B. Deveaud, *The Physics of Semiconductor Microcavities* Wiley-VCH, New York, 2007.
 - [7] O. A. Egorov, D. V. Skryabin and F. Lederer, *Phys. Rev. B* **84**, (2011) 165305.
 - [8] O. A. Egorov, D. V. Skryabin and F. Lederer, *Phys. Rev. B* **82**, (2010) 165326.
 - [9] A. J. Shields, *Nature Photonics* **1**, (2007) 215.
 - [10] S. Ghosh W. H. Wang, F. M. Mendoza, R. C. Myers, X. Li, N. Samarth, A. C. Gossard and D. D. Awschalom, *Nature Materials* **5**, (2006) 261.
 - [11] S. Abdel-Khalek, S. Barzanjeh, H. Eleuch, *International Journal of Theoretical Physics* **50**, (2011) 2939.
 - [12] T. C. H. Liew, I. A. Shelkhy and G. Mapluech, *Physica E* **43**, (2011) 1543.
 - [13] A. Amo, T. C. H. Liew, C. Adrados, R. Houdré, E. Giacobino, A. V. Kavokin and A. Bramati, *Nat. Photon.* **4**, (2010) 361.
 - [14] A. Muller, W. Fang, J. Lawall, and G. S. Solomon, *Phys. Rev. Lett.* **101**, (2008) 027401.

- [15] M. Wagner, H. Schneider, D. Stehr, S. Winnerl, A. M. Andrews, S. Schartner, G. Strasser, and M. Helm, *Phys. Rev. Lett.* **105**, (2010) 167401.
- [16] A. Quattropani, P. Schwendimann, *Phys. Stat. Sol. B* **242**, (2005) 2302.
- [17] E. Giacobino, J.-P. Karr, A. Baas, G. Messin, M. Romanelli, A. Bramati, *Solid Stat. Commun.* **134**, (2005) 97.
- [18] E. Giacobino, J.-P. Karr, G. Messin, H. Eleuch, A. Baas, *C. R. Physique* **3**, (2002) 41.
- [19] G. Messin, J.-P. Karr, H. Eleuch, J. M. Courty and E. Giacobino, *J. Phys. : Condens. Matter* **11**, (1999) 6069.
- [20] H. Eleuch, J. M. Courty, G. Messin, C. Fabre and E. Giacobino, *J. Opt. B. : Quantum Semiclass. Optics* **1**, (1999) 1.
- [21] J. P. Karr, A. Baas, R. Houdré, and E. Giacobino, *Phys. Rev. A* **69**, (2004) 031802.
- [22] A. Baas, J. Ph. Karr, H. Eleuch, and E. Giacobino, *Phys. Rev. A* **69**, (2004) 023809.
- [23] T. K. Paraso, M. Wouters, Y. Léger, F. Morier-Genoud, and B. Deveaud-Plédran, *Nature Materials* **9**, (2011) 655.
- [24] E. A. Cotta and F.M. Matinaga, *Phys. Rev. B* **76**, (2007) 073308.
- [25] J. E. Perreira, P. L. Saldanha, and M. C. Nemes, *J. Appl. Phys.* **110**, (2011) 013104.
- [26] R. Benzi, A. Sutera and A. Vulpiani, *J. Phys. A* **14**, (1981) L453.
- [27] C. Nicolis and G. Nicolis, *Scholarpedia*, **2(11)**, (2007) 1474.
- [28] A. Córdoba, M. C. Lemos, and F. Jiménez-Morales *J. Chem. Phys.* **124**, (2006) 014707.
- [29] I. Z. Kiss and J. L. Hudson, *Phys. Rev. E* **64**, (2001) 046215.
- [30] C. Grebogi, E. Ott, S. Pelikan and J. A. Yorke, *Physica D*, **13**, (1984) 261.
- [31] A. Prasad, S. S. Negi, and R. Ramaswamy, *Int. J. Bif. and Chaos* **11**, (2001) 291.
- [32] A. Prasad, A. Nandi and R. Ramaswamy, *Int. J. Bif. and Chaos* **17**, (2007) 3397.
- [33] M. Tabor, *Chaos and Integrability in Nonlinear Dynamics: An Introduction*, Wiley, New York 1989.
- [34] K. Kaneko, *Collapse of tori and genesis of chaos in dissipative systems*, World Scientific Publication, Singapore, 1986.
- [35] D. Ruelle and F. Takens, *Commun. Math. Phys.* **20**, (1971) 167.
- [36] H. G. Schuster and W. Just, *Deterministic Chaos: An Introduction*, Wiley-VCH Weinheim, 2005.
- [37] J. C. Alexander, J. A. Yorke, Z. You, and I. Kan, *Int. J. Bif. Chaos* **2**, (1992) 795.
- [38] J. F. Heagy, T. L. Carroll, and L. M. Pecora, *Phys. Rev. Lett.* **73**, (1994) 3528.
- [39] P. Ashwin, J. Buescu, and I. N. Stewart, *Phys. Lett. A* **193**, (1994) 126.
- [40] Y. C. Lai and R. L. Winslow, *Phys. Rev. Lett.* **72**, (1994) 1640.
- [41] R. Houdre, C. Weisbuch, R. P. Stanley, U. Oesterle, and M. Ilegems, *Phys. Rev. Lett.* **85**, (2000) 2793.
- [42] H. Haug, *Z. Phys. B* **24**, (1976) 351.
- [43] E. Hanamura, *J. Phys. Soc. Jpn.* **37**, (1974) 1545.
- [44] E. Hanamura, *J. Phys. Soc. Jpn.* **37**, (1974) 1553.
- [45] T. B. Norris, J.-K. Rhee, C.-Y. Sung, Y. Arakawa, M. Nishioka and C. Weisbuch, *Phys. Rev. B* **50**, (1994) 14663.
- [46] C. Ciuti, P. Schwendiman, B. Deveaud, and A. Quattropani, *Phys. Rev. B* **62**, (2000) 4825.
- [47] C. Ciuti, V. Savona, C. Piermarocchi, and A. Quattropani, *Phys. Rev. B* **58**, (1998) 7926.
- [48] B. Sermage, S. Long, I. Abram, J. Y. Marzin, J. Bloch, R. Planel, and V. Thierry-Mieg, *Phys. Rev. B* **53**, (1996) 16516.
- [49] H. Eleuch *Eur. Phys. J. D* **49**, (2008) 391.
- [50] H. Eleuch *Eur. Phys. J. D* **48**, (2008) 139.
- [51] W. H. Press, S. A. Teukolsky, W. T. Vetterling, and B. P. Flannery, *Numerical Recipes: The Art of Scientific Computing*, Cambridge University Press, New York 1986.
- [52] In this work we study only the case where the perturbation frequency $\Omega = 1$. However the transitions are similar for other values of Ω (e.g. 1.5 and 2) as well as for the case where the perturbation frequency is resonant to the Rabi frequency $\Omega = 2g = 3$. The other dynamics, such as strange nonchaotic attractor [30–32] due to irrational frequency, will be reported latter.

Figure captions:

Fig.1 (Color online) Case-I: $\Delta_a = \Delta_b = 0$. (a) The two largest Lyapunov Exponents with function of forcing strength f . Middle row: intensities I_a (black-solid line) and I_b (red-dashed line) as a function of time at different values of the forcing strengths (b) $f = 0.1$ (period-one motion) (c) $f = 0.804$ (period-six motion) (d) $f = 0.329$ (quasiperiodic motion) and (e) $f = 0.5$ (chaotic motion). The scale of y-axes in b), c), d), and e) are the same. The (f), (g), (h) and (i) are the Poincaré section at $Re < a > = 0$ in the intensities space $I_a - I_b$ for b), c) d) and e) respectively. The dotted line in a) represents the zero Lyapunov Exponent. The inset figures are the expanded regions near to different transitions as indicated by arrows.

Fig.2 (Color online) (a) The two largest Lyapunov Exponents and (b) the bifurcation diagram, $Re < a >_m$ (maxima of $Re < a >$) as a function of the forcing strength f near to the marked transition F_2 of Fig. 1(a). The inset figure in b) is expanded region of dotted box.

Fig.3 (Color online) Case-II: $\Delta_a = \Delta_b = g$. The two largest Lyapunov Exponents as a function of the forcing strength f . Middle row: intensities I_a (black-solid line) and I_b (red-dashed line) as a function of time at different forcing strengths (b) $f = 0.006$ (periodic motion) (c) $f = 0.18$ (quasiperiodic motion) and (d) $f = 0.8$ (chaotic motion). The (e), (f) and (g) are the Poincaré section at $Re < a > = 0$ in intensities space $I_a - I_b$ for b), c) and d) respectively. The dotted line in a) represents the zero Lyapunov Exponent.

Fig.4 (Color online) Case-III: $\Delta_a = \Delta_b = -g$. The largest two Lyapunov Exponents as a function of the forcing strength f . Middle row: I_a (black-solid line) and I_b (red-dashed line) as a function of time at forcing strengths (b) $f = 0.5$ (periodic motion) and (c) $f = 1.7728$ (chaotic motion). The (d) and (e) are the Poincaré section at $Re < a > = 0$ in intensity space $I_a - I_b$ for b) and c) respectively. The dashed line in a) corresponds to the zero Lyapunov Exponents. The inset figures in a) and e) are the expanded regions of marked boxes in the respective figures with more data points.

Fig 5 (Color online) Case-III: $\Delta_a = \Delta_b = -g$. The presence of coexisting attractors (a) period and (b) chaotic as function of time at a forcing strength $f = 1.77273$. (c) Then basin of these coexisting attractors in $Re < a >$ vs $Im < a >$ with fixed $Re < b > = Im < b > = 0$. (d) is an expanded basins of marked box in c). (e) shows the fraction of uncertain parameter pairs (out of a sample of 300) as a function of the parameter perturbation δ (see text for detail).

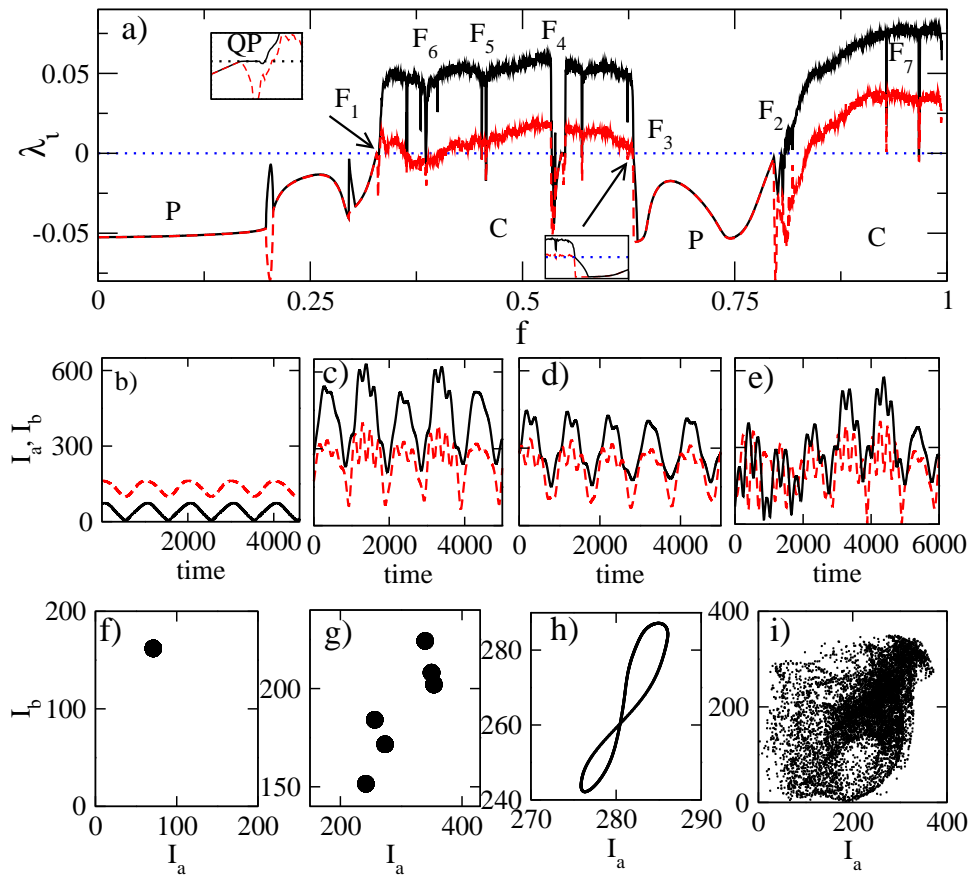


FIG. 1:

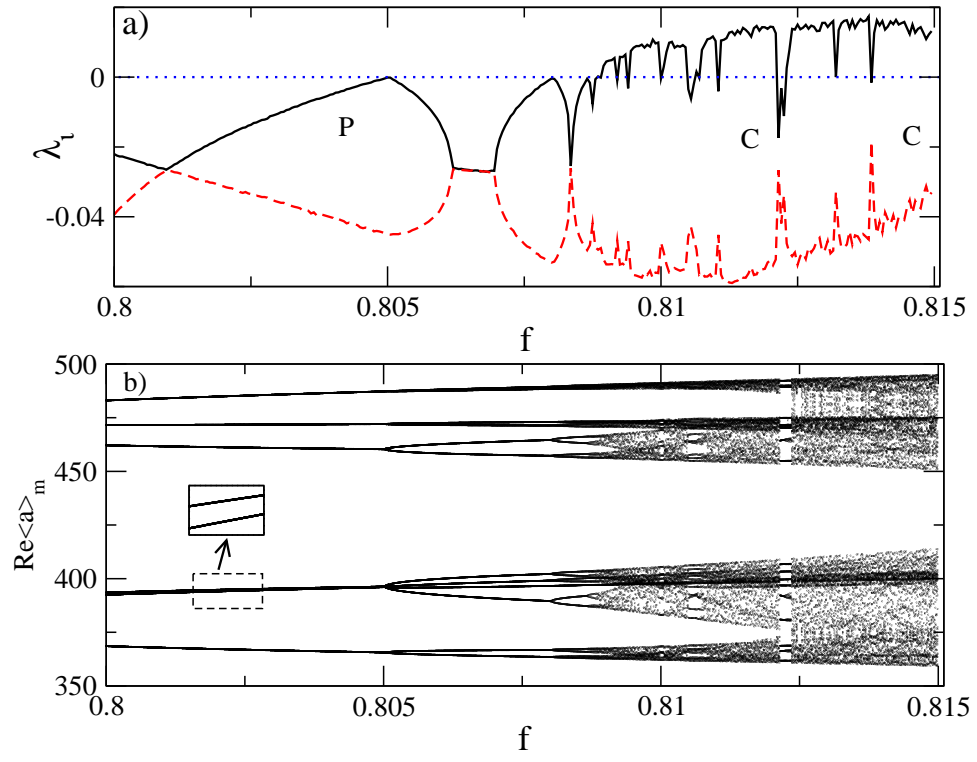


FIG. 2:

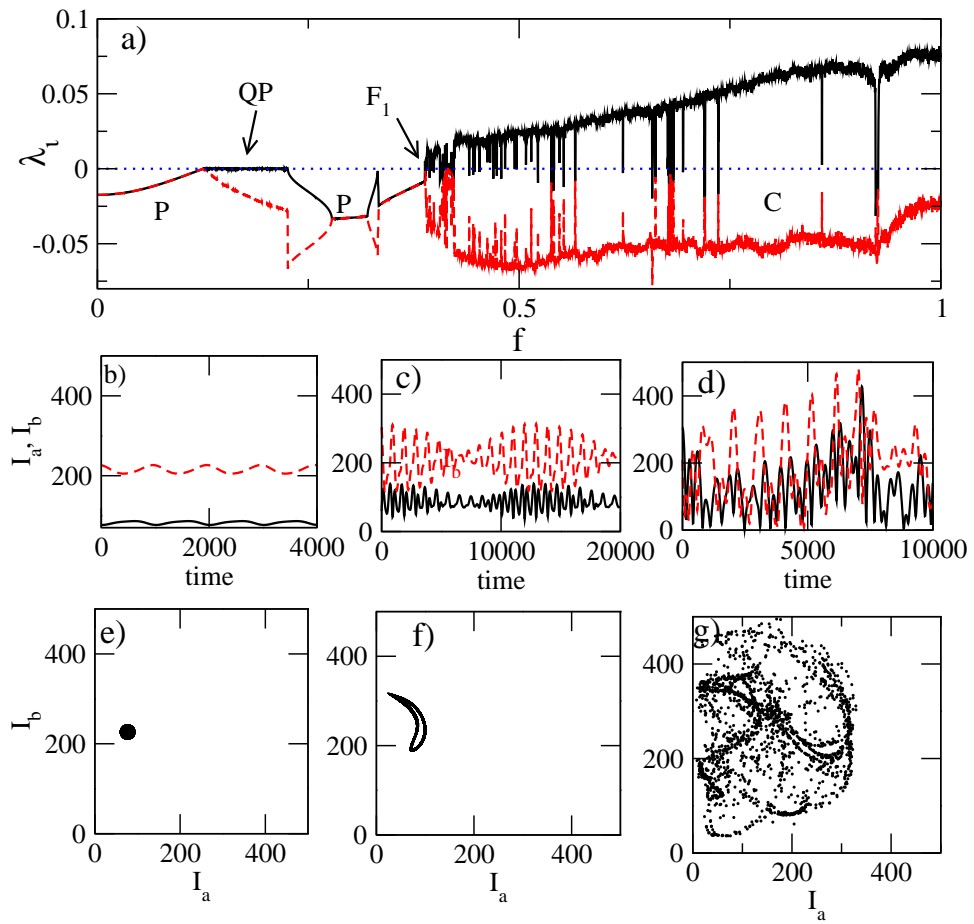


FIG. 3:

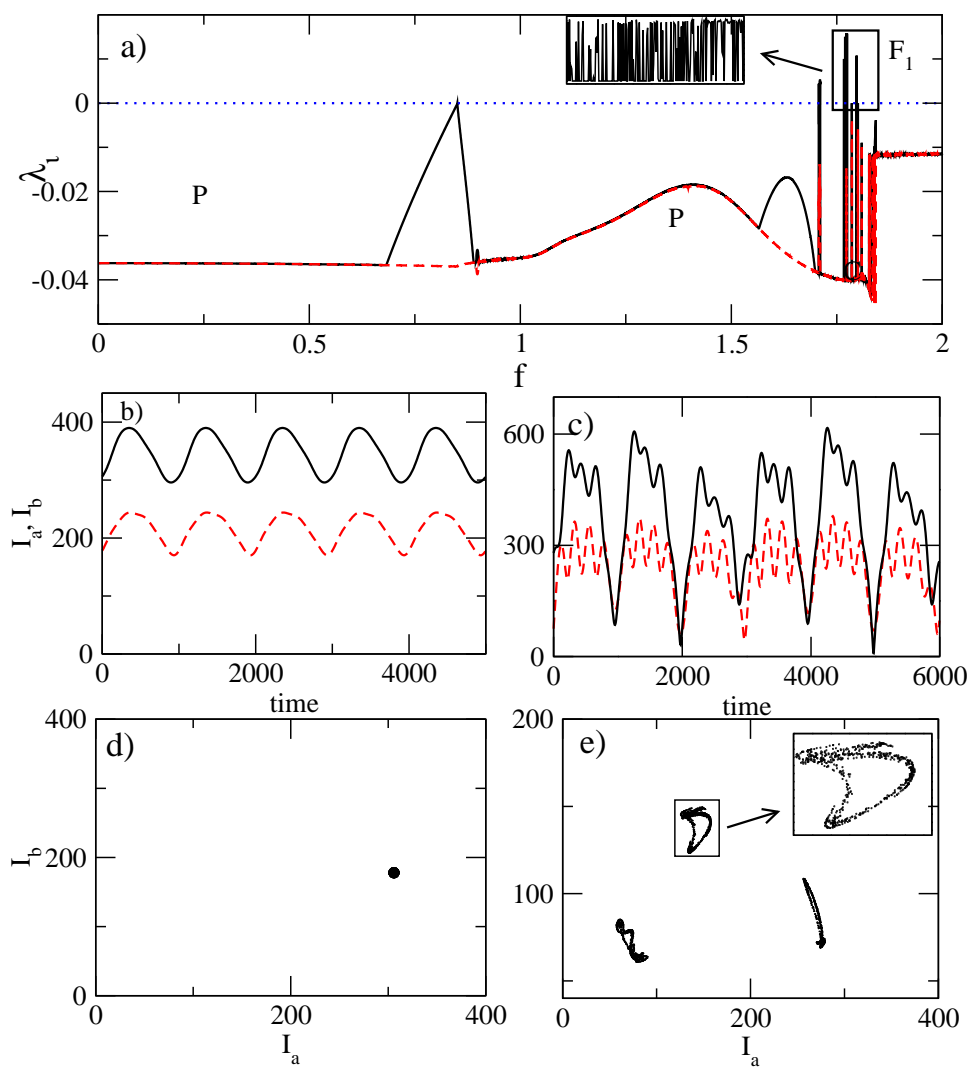


FIG. 4:

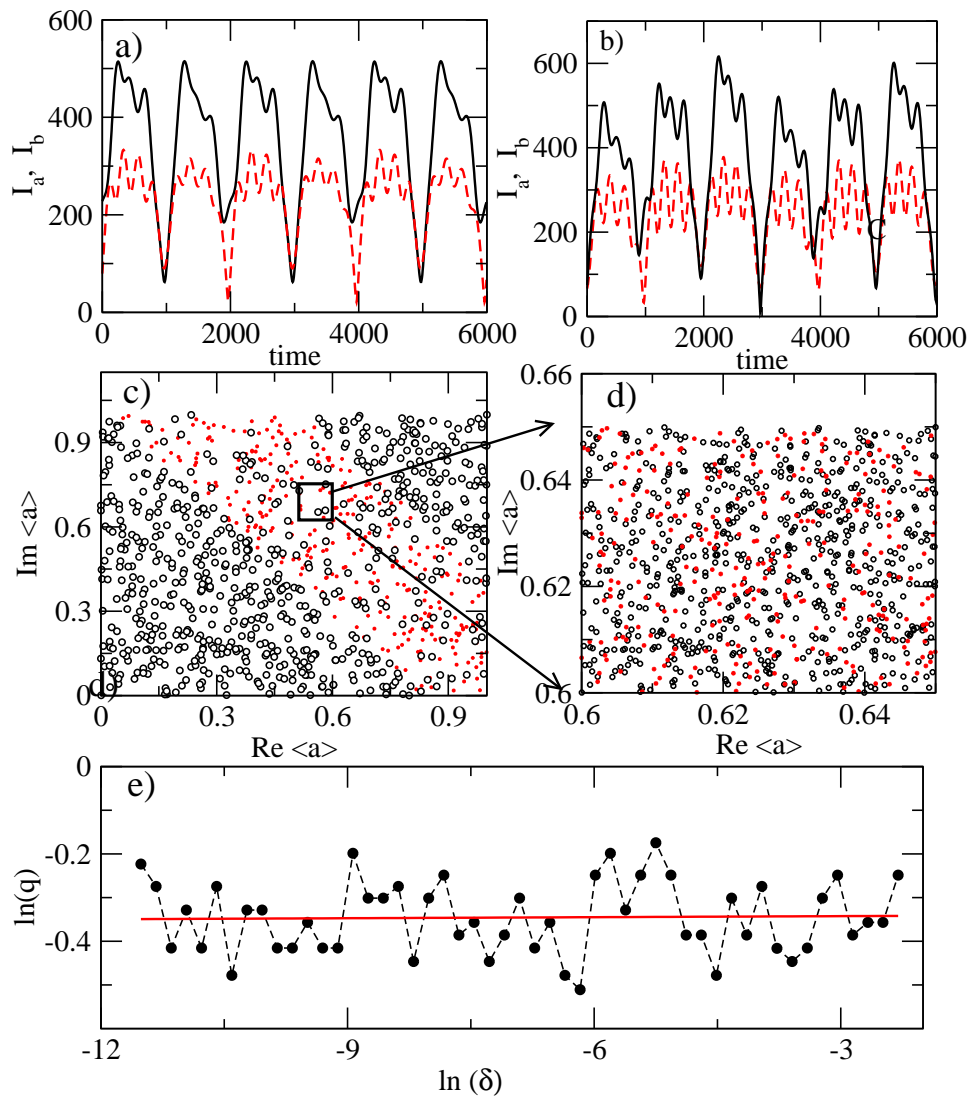


FIG. 5: